

Determination of Reaction Intermediate Structures in Heme Proteins

Kelvin Chu

Summary

Developments in structural biology and molecular biology have allowed increasingly detailed investigations of structure–function relationships. Although atomic-resolution structures of proteins are becoming more common, a growing number of structural studies have focused on the role played by dynamics and have sought to determine the structure of intermediates in protein reactions. These experiments have revealed the first atomic-level pictures of enzyme catalysis and the conformational motions required for biological function. This chapter uses the cryotrapping of reaction intermediates in horse heart myoglobin (Mb) to illustrate the methods utilized in determining the structures of reaction intermediates in protein systems. The techniques described here are applicable to a wide variety of heme proteins including Mb, hemoglobin, photosynthetic reaction centers, and cytochrome p450cam.

Key Words: Myoglobin; cytochrome p450; heme proteins; reaction intermediates; cryotrapping.

1. Introduction

Developments in structural biology and molecular biology have allowed increasingly detailed investigations of structure–function relationships. A growing number of structural studies have focused on the role played by dynamics and have sought to determine the structure of intermediates in protein reactions. These experiments have revealed the first atomic-level pictures of enzyme catalysis and the conformational motions required for biological function (*1–13*). Here, we use the cryotrapping of reaction intermediates in horse heart myoglobin (Mb) to illustrate the methods utilized in determining the structures of reaction intermediates in protein systems. The techniques described here are applicable to a wide variety of heme proteins including Mb (*14–17*), hemoglobin (*18*), photosynthetic reaction centers (*19*), and cytochrome p450cam (*20*).

Examples of studies of reaction intermediates using structural techniques include the rapid trapping of intermediates in isocitrate dehydrogenase from *Escherichia coli* (21), the self-cleavage reaction in RNA catalysis in the hammerhead ribozyme (22), intermediates in the photocycles of photoactive yellow protein (23–25) and bacteriorhodopsin (8–13,26,27), cryotrapping and isolation of the intermediates along the catalytic pathway of cytochrome p450cam from *Pseudomonas putida* (20), ligand migration through Mb (16,20,28), oxygen activation in cytochrome *cdl* nitrite reductase (14), the nucleotidyl transferase pathway of DNA polymerase β (29), and deacylation in a serine protease (30).

Other techniques have been used to investigate systems that are inaccessible to X-ray studies. Electron crystallography has been used to determine the structure of the N intermediate in the bacteriorhodopsin photocycle (27) and the mechanism of proton translocation (26). Three-dimensional nuclear magnetic resonance has been used to examine the structure of the aspartyl-phosphorylation switch in the bacterial enhancer-binding protein NtrC under steady-state phosphorylation conditions (31).

These studies provide the foundation for interpreting biochemical and biophysical data and have been used to elucidate mechanisms of enzyme action (32), laying the groundwork for further study by mutagenesis and computation. We describe the materials and methods for characterization of the reaction intermediates in Mb. Because experimental protocols are crucial in the kinetic characterization of intermediates, we present a detailed rationale for sample treatment and preparation.

2. Materials

2.1. Crystallization of Mb

1. Horse heart Mb (Sigma, St. Louis, MO).
2. 1.7–1.8 M Ammonium sulfate solution.
3. 0.1 M Tris-HCl solution, pH 7.5.
4. 3.4–3.6 M Ammonium sulfate solution.
5. 0.1 M Tris-HCl solution, pH 7.4.
6. 50 mM Sodium dithionite solution.
7. 70 mM Potassium phosphate solution.
8. Hanging-drop crystallization trays (Hampton Research, Alisa Viejo, CA).
9. Carbon monoxide gas (Merriam-Graves, Springfield, MA).
10. Liquid nitrogen.

2.2. Experimental Equipment

1. Microspectrophotometer (32).
2. Open flow helium cryostream capable with temperature control (*see Subheading 3.2.*).
3. 500 mW Argon ion laser (National Laser Company, Salt Lake City, UT).

4. CryoCap system and crystal handling tools (Hampton Research).
5. Fiber optic illuminator (Oriel, Stratford, CT).
6. O₂ pressure cell for crystallography (33).

3. Methods

The methods following the outline: (1) the crystallization of horse heart Mb, (2) characterization of the protein, (3) the preparation of ultra-low temperature cryocrystallography, and (4) data collection strategies.

3.1. Crystallization of Mb and Derivatives

Horse heart Mb is crystallized at room temperature by equilibrating 10-mL drops of 5 mg/mL protein in 1.7–1.8 M ammonium sulfate and 0.1 M Tris-HCl, pH 7.5, against 1 mL of 3.4–3.6 M ammonium sulfate and 0.1 M Tris-HCl, pH 7.4, using the hanging-drop geometry. Crystals should appear within several days with rosette-shaped crystals within 2 wk. Leaflets from the crystals can be harvested from the rosettes using Hampton Microtools. Typical sizes of crystals are 0.01 × 0.07 × 0.3 mm. These crystals are high-spin iron (*met*, Fe^{III}) and should appear brown. Crystals are typically P21 with characteristic unit cell dimensions of $a = 63.6 \text{ \AA}$, $b = 28.8 \text{ \AA}$, $c = 35.6 \text{ \AA}$, and $\beta = 106.5 \text{ \AA}$ (28,34). These crystals are the starting point for preparation of ligand derivatives:

1. Ferrous unligated Mb crystals are obtained by soaking *met* crystals in a nitrogenated solution containing 50 mM sodium dithionite, 70 mM potassium phosphate, and 70% saturated ammonium sulfate. The color of the crystals should change from brown to bright red. Deoxy Mb crystals should be flash frozen quickly in liquid nitrogen to prevent O₂ substitution from the atmosphere.
2. Ferrous CO-bound crystals are obtained by soaking *met* crystals in CO-saturated mother liquor supplemented by 8 mg/mol dithionite, 5 mL 2 M NaOH/mL, and 7.5% glycerol. The color of the crystals should change from brown to raspberry red over the period of 30 min. MbCO crystals should be flash frozen immediately in liquid nitrogen to prevent auto-oxidation.
3. Ferrous O₂-bound crystals are obtained by soaking *met* crystals in a solution of 50 mM potassium phosphate at pH 7.0, 70% saturated ammonium sulfate, 10% glucose (w/v), and 10% sucrose (w/v). Crystals are transferred into a pressure chamber and exposed to 100 bar of O₂ for 30 min at 4°C. Once ligated, pressure should be released from the chamber slowly (over tens of seconds) to prevent flash cooling from rapid depressurization. MbO₂ crystals should be flash frozen immediately in liquid nitrogen to prevent auto-oxidation.

3.2. Characterization of Intermediates

Structural characterization of reaction intermediates relies on independent confirmation of the nature of the intermediate, often by spectroscopy (35). In addition, the nature of this identification is often *kinetic* as opposed to purely

spectroscopic. Because protein chromophores are often not sensitive to the ligand position in the protein, many studies have therefore relied on infrared spectroscopy in addition to UV/Vis spectroscopy, using the dipole absorption of the ligand in the infrared. The transient nature of intermediates in a protein reaction means that two techniques must be added to conventional structure determination: initiation of the reaction and sufficient accumulation of the reaction in crystals (35,36). These techniques must be efficient, not overly damage the sample or radically change the kinetic properties of the system, and must be rapid compared with the time-scale of the reaction being studied (36).

3.2.1. Reaction Initiation

For Mb, the initiation of the reaction is accomplished by photolysis. Carbon monoxide is used as a ligand because although it is similar in many respects to O₂, the quantum yield for photolysis is unity. Time-resolved spectroscopic measurements and molecular dynamics simulations show that ligand rebinding in MbCO occurs in two sequential intermediates resulting from both movement of the ligand within the protein matrix and conformational relaxation of the protein.

Spectroscopic studies indicate that following dissociation, the spectrum of free CO appears in approx 0.5 ps and persists for hundreds of nanoseconds (37). The extent of geminate, or internal, recombination from this site depends on the reactivity of the ligand with the heme iron and its ability to diffuse away from the active site to a secondary docking site (D) or the solvent (S). The latter process requires relatively large anharmonic protein fluctuations on a microsecond time-scale that are frozen out below the glass-transition temperature, around 180K (38). The general scheme is shown in **Table 1**.

3.2.2. Accumulation of Intermediates

To observe intermediates crystallographically, one must accumulate roughly 30% occupancy in the experiment. Separate protocols that can distinguish between the B and D intermediates must be designed. Temperature-derivative spectroscopy (TDS), a technique adapted from low-temperature solid-state physics (39) is used to design the protocol for characterization of intermediates. In a typical experiment, the reaction is initiated and the temperature is ramped up linearly in time while spectra are collected for each Kelvin temperature increase. This procedure effectively sweeps thermally activated processes through the window of observable rates of the instrument.

The structural heterogeneity in the sample results in a distribution of rates. At low temperatures, only processes with low barriers for recombination can rebind within the time window of the spectrometer. Differences between spectra from consecutive temperatures are plotted as a contour plot of population or change in absorbance as a function of wavenumber and rebinding enthalpy (**Fig. 1**). As the

Table 1
Reaction Scheme for Carbonmonoxymyoglobin^a

Reaction	MbCO	↔	Mb*CO	↔	Mb**CO	↔	Mb + CO
State:	A		B		D		S
Name:	(bound)		(photolyzed)		(photorelaxed)		(deoxy)
Ligand position	Heme		1° site		2° site		solvent

^aPhotolysis protocols can drive the ligand to either state B (photolyzed) or state D (photorelaxed), depending on the temperature profile of the sample. Rebinding from B⇒A or B⇒D occurs sequentially. Enthalpies for rebinding are determined using temperature-derivative spectroscopy. $H_{BA} \sim 12$ kJ/mol, $H_{DA} \sim 30$ kJ/mol.

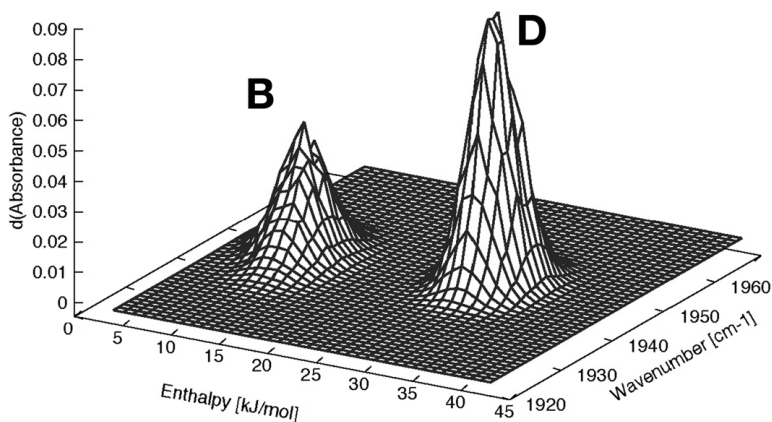


Fig. 1. Temperature-derivative spectroscopy plot for hMbCO. This plot reveals the rationale for design of the experiment. Samples photolyzed at 10K will generate only proteins in the B state. Samples cooled under illumination will generate both states B and D. However, collecting data at 90K allows rebinding of the B state, leaving the only nonligated CO molecules in the D position.

temperature is increased, individual ligand molecules gain sufficient energy to overcome higher barriers and recombine. Thus, TDS sorts different rate processes according to their activation enthalpy. The relation between enthalpy and peak rebinding temperature are related if we assume a first-order rate process,

$$\frac{dN}{dt} = -kN \quad (1)$$

and an Arrhenius-like rate,

$$k = A \left(\frac{T}{T_0} \right) \exp \left(-\frac{H}{RT} \right) \quad (2)$$

where A is the pre-exponential at the arbitrary reference temperature T_0 , H is the height of the enthalpic barrier, R is the gas constant, and T is the temperature (Kelvin). The measured TDS signal can be then written as

$$\frac{dN}{dT} = -\frac{N_0}{\beta} \int_0^\infty k \exp\left(-\int_{T_0}^T \frac{k}{\beta} dT\right) g(H) dH \quad (3)$$

The characteristic time for the measurement, τ_c , is given by

$$\tau_c = \frac{RT_p^3}{\beta T_p (H + RT_p)} \quad (4)$$

where the peak enthalpy is

$$H_p = T_p R \ln(A \tau_c) \quad (5)$$

Laser irradiation is used to enhance a particular photoproduct species, a process called pumping. Samples cooled under illumination undergo continuous photolysis while the temperature is ramped from 160 to 10K. The range of accessible conformational motions is frozen out as the sample cools, trapping long-lived states.

A TDS plot for hMbCO is shown in **Fig. 1**. Data are presented as a surface plot (or a contour plot) of population as a function of wavelength and rebinding enthalpy. Large signals (peaks) indicate increases in rebinding population for a particular wavelength and a particular rebinding enthalpy. Flat areas indicate no rebinding occurs.

3.3. Ultra-Low Temperature Crystallography

Crystallographic determination of structures of reaction intermediates relies on either rapid collection via the Laue diffraction or stabilization of intermediates on time-scales suitable for monochromatic data collection (**40–42**). The latter can be done chemically (e.g., by modification of the macromolecule, substrate, cofactor, solvent, or pH) or physically (by temperature) (**43,44**). Because most single-protein crystals are commonly flash cooled for stabilization during data collection to slow radiation damage, trapping intermediates by freeze quenching a reaction is very common.

Metalloporphyrin proteins often have a relatively large heme pocket designed to accommodate ligands, as in the case of hemoglobin or Mb, or large substrates, as in cytochrome P450cam. This results typically in a fast-rebinding geminate phase in flash-photolysis studies of heme protein kinetics, corresponding to low enthalpic barriers for rebinding (~ 4 kJ/mol) following photolysis. To adequately trap suitable populations of ligands in these low enthalpic barrier states, correspondingly low temperatures must be used. For Mb and hemoglobin, liquid helium temperatures are employed to slow recombination.

We have designed a helium cryostream that consists of a liquid helium stream for cooling the crystal and an exterior, concentric flow of warm, room-temperature gas (*see Note 1*). The gas flow rate of the inner stream is controlled by the needle valve of a liquid helium transfer line (Janis) (*see Note 2*). The regulator from a cylinder of helium gas controls the gas flow rate of the outer stream (*see Note 3*). Recently, cryostreams from commercial suppliers have become available. These ultra-low temperature cryostreams employ displacer refrigerators for cooling, and need no cryogenic liquids.

3.4. Data Collection

3.4.1. Mb*CO (B) Structure

To determine the structure of the Mb*CO complex, crystals are photolyzed at helium temperatures to slow the rebinding reaction to experimentally convenient time-scales for monochromatic data collection. Experiments are aimed at optimizing the population of the D intermediate. Cryocooling prevents the escape of the photolyzed CO to the solvent.

Steps in data collection are:

1. Prepare MbCO crystals as described in **Subheading 3.1.** and mount crystals directly in the loop of a CryoCap.
2. Freeze the crystals directly in the helium stream. Note that prefreezing in liquid nitrogen is not possible.
3. Illuminate the crystal with low-intensity light, such as a fiber-optic illuminator (*see Note 4*). Collection of data should be performed with the illumination light on. Rebinding is non-negligible at helium temperatures and molecular tunneling of the CO can occur even at 4.2K, so samples should be under continuous illumination at low power during data collection. Simultaneously, too high an illumination will result in significant crystal heating and increased recombination (*17*).

3.4.2. Mb**CO (D) Structure

The D intermediate requires relaxation of the protein. This occurs thermally at room temperature for native Mb with around 10% occupancy. Cryotrapping of the D state is required to accumulate sufficient amounts of the intermediate for structural determination by X-ray crystallography. For data collection of the photorelaxed hMb**CO complex, the crystal should be illuminated with an argon ion laser at a relatively high temperature (160–180K) and then cooled under illumination to 90–100K for trapping at a rate of 10K/h.

Steps in data collection are:

1. Prepare MbCO crystals as described in **Subheading 3.1.** and mount crystals directly in the loop of a CryoCap.
2. Freeze the crystals directly in a nitrogen stream.

3. Illuminate crystals with an argon ion laser (*see Note 5*). To ensure homogeneous illumination conditions, illuminate both sides of the flat surface of the leaflet for 6 h at 160K with an intensity of roughly 5 mW/mm².
4. Cool the crystal under illumination at 10K/h to 85K. Excessive illumination will cause heating of the sample. Temperature fluctuations on the order of 5K will result in significant rebinding during the experiment.

4. Notes

1. Despite the best alignment of cold and warm gas streams, turbulence and pressure regulation problems may eventually generate sufficiently nonlaminar flow so that moisture from ambient air will reach the cold helium stream and condense. This icing can be diminished by construction of small Kapton shields that extend over the CryoCap pin.
2. We have measured the temperature profile of the helium stream using a silicon diode mounted on a goniometer loop and found that crystallography at liquid helium temperatures requires much more precision in positioning of cryostream position with respect to the goniometer geometry. This is because the specific heat of helium is much lower than that of nitrogen, and, thus, the cooling power of the helium cryostream is greatly reduced. The typical protocol for cryostream positioning is to move the cryostream tip as close to the sample as possible without eclipsing high-resolution data. We use a very narrow cryostream tip (1.5-mm diameter) and typically have distances between the cryostream tip and the sample of less than 3 mm.
3. Obviously, samples should not be directly manipulated by hand when they are in the helium cryostream. When using prefrozen crystals, we have had good results with cryotongs that have been modified for the tight helium cryostream geometry. If, when mounting, nitrogen from LN2 freezes on the sample, it can be gently removed by direct manipulation with an unused cryoloop.
4. Heating from the photolysis and illumination beams can be significant. For photolysis, low-intensity illumination protocols should be used; heating in excess of 10–20°C occurs with direct illumination with a laser. If monochromatic illumination must be used, a standard trick is to choose a long wavelength where the crystal appears optically less thick. This strategy has been successfully employed by time-resolved studies.
5. Steps should be taken to ensure that photoselection does not occur during illumination. If a polarized light source is used for illumination and photolysis, it should not rotate with the crystal.

Acknowledgments

Thanks to Ilme Schlichting and Hans Frauenfelder for stimulating discussions. This work was supported by grants from the National Science Foundation, the Research Corporation, and the Petroleum Research Fund.

References

1. Stoddard, B. L. (1998) New results using Laue diffraction and time-resolved crystallography. *Curr. Opin. Struct. Biol.* **8**, 612–618.
2. Ridder, I. S., Rozeboom, H. J., Kalk, K. H., and Dijkstra, B. W. (1999) Crystal structures of intermediates in the dehalogenation of haloalkanoates by L-2-haloacid dehalogenase. *J. Biol. Chem.* **274**, 30,672–30,678.
3. Pannifer, A. D., Flint, A. J., Tonks, N. K., and Barford, D. (1998) Visualization of the cysteinyl-phosphate intermediate of a protein-tyrosine phosphatase by x-ray crystallography. *J. Biol. Chem.* **273**, 10,454–10,462.
4. Burzlaff, N. I., Rutledge, P. J., Clifton, I. J., et al. (1999) The reaction cycle of isopenicillin N synthase observed by X-ray diffraction. *Nature* **401**, 721–724.
5. Ogle, J. M., Clifton, I. J., Rutledge, P. J., et al. (2001) Alternative oxidation by isopenicillin N synthase observed by X-ray diffraction. *Chem. Biol.* **8**, 1231–1237.
6. Wilmot, C. M., Hajdu, J., McPherson, M. J., Knowles, P. F., and Phillips, S. E. (1999) Visualization of dioxygen bound to copper during enzyme catalysis. *Science* **286**, 1724–1728.
7. Murray, J. B., Szoke, H., Szoke, A., and Scott, W. G. (2000) Capture and visualization of a catalytic RNA enzyme-product complex using crystal lattice trapping and X-ray holographic reconstruction. *Mol. Cell.* **5**, 279–287.
8. Kuhlbrandt, W. (2000) Bacteriorhodopsin—the movie. *Nature* **406**, 569–570.
9. Luecke, H., Schobert, B., Richter, H. T., Cartailler, J. P., and Lanyi, J. K. (1999) Structural changes in bacteriorhodopsin during ion transport at 2 angstrom resolution. *Science* **286**, 255–261.
10. Luecke, H., Schobert, B., Richter, H. T., Cartailler, J. P., and Lanyi, J. K. (1999) Structure of bacteriorhodopsin at 1.55 Å resolution. *J. Mol. Biol.* **291**, 899–911.
11. Edman, K., Nollert, P., Royant, A., et al. (1999) High-resolution X-ray structure of an early intermediate in the bacteriorhodopsin photocycle. *Nature* **401**, 822–826.
12. Royant, A., Edman, K., Ursby, T., Pebay-Peyroula, E., Landau, E. M., and Neutze, R. (2000) Helix deformation is coupled to vectorial proton transport in the photocycle of bacteriorhodopsin. *Nature* **406**, 645–648.
13. Sass, H. J., Buldt, G., Gessenich, R., et al. (2000) Structural alterations for proton translocation in the M state of wild-type bacteriorhodopsin. *Nature* **406**, 649–653.
14. Chu, K., Vojtechovsky, J., McMahon, B. H., Sweet, R. M., Berendzen, J., and Schlichting, I. (2000) Structure of a new ligand-binding intermediate in wildtype carbonmonoxymyoglobin. *Nature* **403**, 921–923.
15. Schlichting, I., Berendzen, J., Phillips, G. N., Jr., and Sweet, R. M. (1994) Crystal structure of photolyzed myoglobin. *Nature* **371**, 808–812.
16. Ostermann, A., Waschipky, R., Parak, F. G., and Nienhaus, G. U. (2000) Ligand binding and conformational motions in myoglobin. *Nature* **404**, 205–208.
17. Teng, T. Y., Srajer, V., and Moffat, K. (1994) Photolysis-induced structural changes in single crystals of carbonmonoxymyoglobin at 40K. *Nat. Struct. Biol.* **1**, 701–705.

18. Adachi, S., Park, S. Y., Tame, J. R., Shiro, Y., and Shibayama, N. (2003) Direct observation of photolysis-induced tertiary structural changes in hemoglobin. *Proc. Natl. Acad. Sci. USA* **100**, 7039–7044.
19. Stowell, M. H., McPhillips, T. M., Rees, D. C., Soltis, S. M., Abresch, E., and Feher, G. (1997) Light-induced structural changes in photosynthetic reaction center: implications for mechanism of electron-proton transfer. *Science* **276**, 812–816.
20. Schlichting, I., Berendzen, J., Chu, K., et al. (2000) The catalytic pathway of cytochrome P450cam at atomic resolution. *Science* **287**, 1615–1622.
21. Stoddard, B. L. (1999) Visualizing enzyme intermediates using fast diffraction and reaction trapping methods: isocitrate dehydrogenase. *Biochem. Soc. Trans.* **27**, 42–48.
22. Scott, W.G. (1999) Biophysical and biochemical investigations of RNA catalysis in the hammerhead ribozyme. *Q. Rev. Biophys.* **32**, 241–284.
23. Genick, U. K., Borgstahl, G. E., Ng, K., et al. (1997) Structure of a protein photocycle intermediate by millisecond time-resolved crystallography. *Science* **275**, 1471–1475.
24. Genick, U. K., Soltis, S. M., Kuhn, P., Canestrelli, I. L., and Getzoff, E. D. (1998) Structure at 0.85 Å resolution of an early protein photocycle intermediate. *Nature* **392**, 206–209.
25. Perman, B., Srajer, V., Ren, Z., et al. (1998) Energy transduction on the nanosecond time scale: early structural events in a xanthopsin photocycle. *Science* **279**, 1946–1950.
26. Subramaniam, S. and R. Henderson (2000) Molecular mechanism of vectorial proton translocation by bacteriorhodopsin. *Nature* **406**, 653–657.
27. Vonck, J. (2000) Structure of the bacteriorhodopsin mutant F219L N intermediate revealed by electron crystallography. *Embo. J.* **19**, 2152–2160.
28. Brunori, M., Vallone, B., Cutruzzola, F., et al. (2000) The role of cavities in protein dynamics: crystal structure of a photolytic intermediate of a mutant myoglobin. *Proc. Natl. Acad. Sci. USA* **97**, 2058–2063.
29. Sjogren, T. and Hajdu, J. (2001) Structure of the bound dioxygen species in the cytochrome oxidase reaction of cytochrome cd1 nitrite reductase. *J. Biol. Chem.* **276**, 13,072–13,076.
30. Arndt, J. W., Gong, W., Zhong, X., et al. (2001) Insight into the catalytic mechanism of DNA polymerase beta: structures of intermediate complexes. *Biochemistry* **40**, 5368–5375.
31. Wilmouth, R. C., Edman, K., Neutze, R., et al. (2001) X-ray snapshots of serine protease catalysis reveal a tetrahedral intermediate. *Nat. Struct. Biol.* **8**, 689–694.
32. Kern, D., Volkman, B. F., Luginbuhl, P., Nohaile, M. J., Kustu, S., and Wemmer, D. E. (1999) Structure of a transiently phosphorylated switch in bacterial signal transduction. *Nature* **402**, 894–898.
33. Hadfield, A. and Hajdu, J. (1994) On the photochemical release of phosphate from 3,5-dinitrophenyl phosphate in a protein crystal. *J. Mol. Biol.* **236**, 995–1000.
34. Urayama, P., Phillips, G. N., and Gruner, S. M. (2002) Probing substates in sperm whale myoglobin using high-pressure crystallography. *Structure* **10**, 51–60.

35. Vojtechovsky, J., Chu, K., Berendzen, J., Sweet, R. M., and Schlichting, I. (1999) Crystal structures of myoglobin-ligand complexes at near-atomic resolution. *Biophys. J.* **77**, 2153–2174.
36. Schlichting, I. and Chu, K. (2000) Trapping intermediates in the crystal: ligand binding to myoglobin. *Curr. Opin. Struct. Biol.* **10**, 744–752.
37. Wilmot, C. M. and Pearson, A. R. (2002) Cryocrystallography of metalloprotein reaction intermediates. *Curr. Opin. Chem. Biol.* **6**, 202–207.
38. Schlichting, I. and Goody, R. S. (1997) Triggering Methods in crystallographic enzyme kinetics. *Meth. Enzymol.* **277**, 467–490.
39. Lim, M., Jackson, T. A., and Anfinrud, P. A. (1997) Ultrafast rotation and trapping of carbon monoxide dissociated from myoglobin. *Nat. Struct. Biol.* **4**, 209–214.
40. Chu, K., Ernst, R.M., Frauenfelder, H., Mourant, J. R., Nienhaus, G. U., and Philipp, R. (1995) Light-induced and thermal relaxation in a protein. *Phys. Rev. Lett.* **74**, 2607–2610.
41. Berendzen, J. and Braunstein, D. (1990) Temperature-derivative spectroscopy: a tool for protein dynamics. *Proc. Natl. Acad. Sci. USA* **87**, 1–5.
42. Petsko, G. A. and Ringe, D. (2000) Observation of unstable species in enzyme-catalyzed transformations using protein crystallography. *Curr. Opin. Chem. Biol.* **4**, 89–94.
43. Schlichting, I. (2000) Crystallographic structure determination of unstable species. *Acc. Chem. Res.* **33**, 532–538.
44. Ursby, T., Weik, M., Fioravanti, E., Delarue, M., Goeldner, M., and Bourgeois, D. (2002) Cryophotolysis of caged compounds: a technique for trapping intermediate states in protein crystals. *Acta Crystallogr. D. Biol. Crystallogr.* **58**, 607–614.

